Structure of a $^4T_2$ level of Mn^{++} in tetrahedral symmetry, dynamical Jahn-Teller effect and selective intensity transfer

R. Parrot, C. Naud, and F. Gendron

Université Pierre et Marie Curie, Laboratoire de Luminescence, Equipe de recherche associée au Centre National de la Recherche Scientifique, 4 place Jussieu, 75230 Paris, Cedex 05, France

(Received 30 January 1975; revised manuscript received 7 July 1975)

An experimental study under uniaxial stresses and a theoretical analysis of the zero-phonon lines of the lowest $^4T_2$ level of Mn^{++} in ZnSe are reported. We first show that a classical model in which vibronic interactions are neglected must be rejected since it predicts a zero-stress spectrum of the zero-phonon lines consisting of three absorption lines with relative dipole strengths of 14, 7, and 9 although only two absorption lines at 19597 and 19607 cm^{-1} are observed. Then, in order to interpret this unusual structure we consider Ham's effect corresponding to Jahn-Teller interactions of the $^4T_2$ electronic state with E vibrational modes. It is shown that the hypothesis of strong Jahn-Teller interactions is consistent with the zero-stress spectrum but inconsistent with pressure-induced splittings and polarizations. Finally a model permitting a correct interpretation of all experimental results has been elaborated by considering a medium coupling to E vibrational modes. We show that the observed lines at 19597 and 19607 cm^{-1} correspond, respectively, to transitions from the $^6A_1$ ground state to the $|\Gamma_8(5/2)\rangle$ and $|\Gamma_6\rangle$ fundamental vibronic levels of the $^4T_2$ state. Furthermore, a careful analysis of the dipole strengths of the zero-phonon lines and phonon-assisted lines shows the importance of intensity transfer from the zero-phonon lines to the phonon-assisted lines. The case of Mn^{++} in ZnS is also briefly considered.

I. INTRODUCTION

Transition-metal ions with a half-filled external shell, and particularly Mn^{++} ions, have been extensively studied during the last two decades. These studies were often concerned with the electronic levels as well as with their interactions with the lattice.

For example, the problem of covalent bondings for Mn^{++} and the interaction of electronic states with odd-parity vibrational states in centrosymmetric complexes have been studied for a long time.[1,2] The relation between covalent bondings and the Jahn-Teller effect have been considered by Lohr.[3] The magnon sidebands and the Jahn-Teller effect on magnon sidebands of Mn^{++} in antiferromagnetic crystals were studied more recently.[4-6] Except for the last example, the fine structure of the optical multiplets did not intervene explicitly in these works.

In numerous studies concerning optical levels of Mn^{++}, the nature of the fine-structure lines was determined by comparing the experimental and theoretical splittings of pure electronic states.[7] However, in the case of Mn^{++} ions, this fitting procedure must be used with caution since, as demonstrated by Solomon and McClure,[5] the Jahn-Teller effect can be of importance.

More specifically, in the case of Mn^{++} in ZnS, some lines appearing in the optical spectra of highly concentrated crystals have been tentatively associated with pair lines,[8] but as demonstrated by Langer and Ibuki[9] most of the lines appearing in the lowest bands of Mn^{++} in ZnS can be associated with zero-phonon and phonon-assisted transitions of noninteracting Mn^{++} ions. However, the spectra are often complicated by the presence of Mn^{++} ions in stacking faults so that it is not a simple matter of recognizing clearly the lines associated with the various centers.[10,11]

Therefore, being interested in the structure of the lowest $^4T_2$ band of Mn^{++}, we studied concomitantly Mn^{++} in ZnS and in ZnSe. The fact that the lines appearing in the $^4T_2$ band of the latter are well resolved was of great help in obtaining clear experimental results under uniaxial stresses and therefore in understanding the structure of the $^4T_2$ zero-phonon lines.

Simple symmetry considerations show that in T_d symmetry a $^4T_2$ level decomposes into four levels, two Kramer's doublets Γ_6 and Γ_7 and two Γ_8 levels [denoted $\Gamma_8(\frac{3}{2})$ and $\Gamma_8(\frac{5}{2})$] (see Fig. 1). For Mn^{++} in ZnSe and ZnS the spectrum of the zero-phonon lines of the $^4T_2$ level is composed of two lines separated, respectively, by 10 and 3 cm^{-1}. (Fig. 2). Thus the first problem encountered was the identification of the observed lines. The uniaxial-stress experiments reported in Sec. II were performed for this purpose.

In Sec. III we recall the classical theory of a triplet state in a static crystal field of T_d symmetry. This theory will permit us to obtain the order of magnitude for the splitting of the lowest $^4T_2$ state of Mn^{++} by spin-orbit interaction. We also set up general formulas permitting the calculation of the relative dipole strengths of the fine-

structure lines for a $^4T_2$ state (these formulas will be used with minor modifications in their interpretation when vibronic interactions are considered). In Sec. III E we show that the two lines observed experimentally could be interpreted as transitions from the $^6A_1$ ground state to a Γ_6 and $\Gamma_8(\frac{5}{2})$ electronic level. However, this classical model is unable to give a correct explanation for the nonobservation of the $^6A_1 \rightarrow \Gamma_8(\frac{3}{2})$ transition.

In an alternate model presented in Sec. IV, we consider the influence of weak and strong vibronic coupling to E vibrational modes and show that the presence of only two lines in the experimental spectra could be due to strong vibronic interactions. However, we show that this model predicts uniaxial-stress effects which are in disagreement with those observed.

Finally, in Secs. V and VI we elaborate a model permitting a correct interpretation of all experimental results. In particular, by carefully analyzing the influence of the vibronic interations on the zero-phonon lines as well as on the phonon-assisted lines, we show the importance of intensity transfer from zero-phonon to phonon-assisted lines.

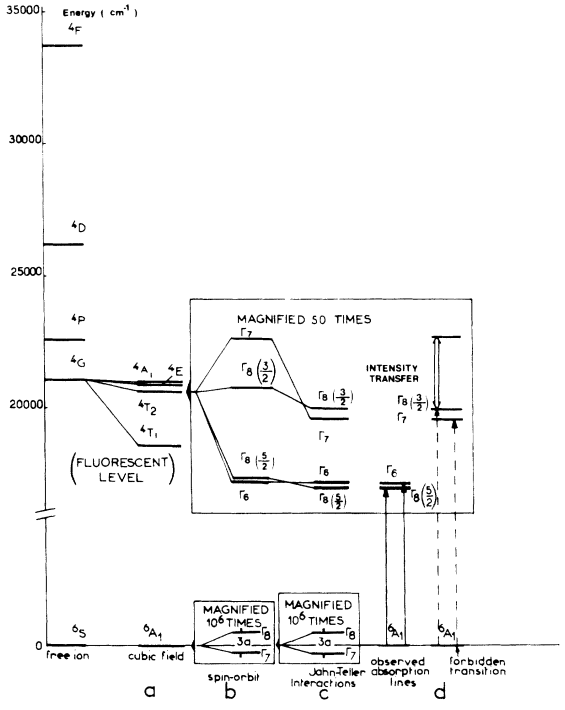

FIG. 1. (a) Lowest energy levels for Mn^{++} in cubic symmetry. (b) Splitting of the $^4T_2$ level due to first- and second-order spin-orbit interactions. (c) Effect of vibronic interactions with an E vibrational mode. (d) Energy levels and intensity transfer predicted by the model of Sec. VI for Mn^{++} in ZnSe and ZnS.

II. EXPERIMENTS

A. Samples and apparatus

The samples of ZnSe:Mn were grown by Semi-elements. The Mn^{++} concentration was 10^{-3} mole%. The samples were cut and mechanically polished. The dimensions of the crystals were as follows: $2.75 \times 1.55 \times 3.60$ mm^3, the surface S perpendicular to the [001] direction being $(1.55 \pm 0.01) \times (2.75 \pm 0.01)$ mm^2; and $2.87 \times 1.93 \times 6.50$ mm^3, the surface S perpendicular to the [110] direction being $(1.93 \pm 0.01) \times (2.87 \pm 0.01)$ mm^2; and $2.70 \times 3.45 \times 3.55$ mm^3, the surface S perpendicular to the [111] direction being $(2.70 \pm 0.01) \times (3.45 \pm 0.01)$ mm^2.

For our experiments on ZnS:Mn we used the single crystals described in a preceding paper.[10] Although these samples possess Mn^{++} centers in stacking faults the zero-phonon lines of the lowest levels of Mn^{++} in cubic and axial sites are sufficiently well known[11] and sufficiently separated for the $^4T_2$ band so as to create no problem in our interpretation. Furthermore, it has been shown

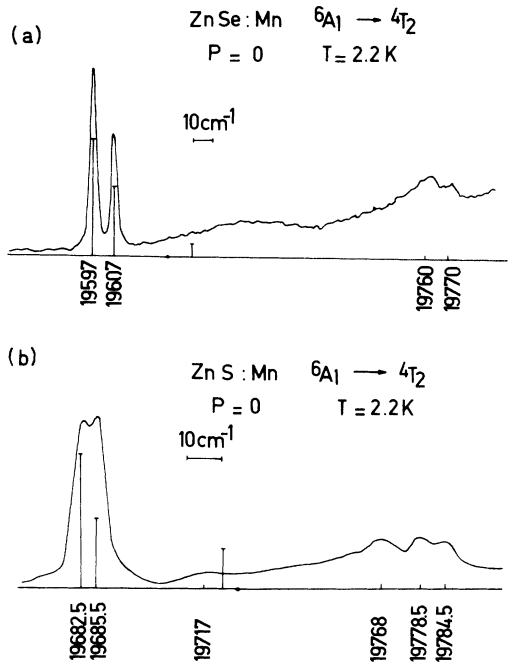

FIG. 2. Spectrometer recordings of the absorption lines appearing in the vicinity of the zero-phonon lines of the $^4T_2$ level for zero applied pressure and calculated positions and dipole strengths resulting from the model given in Sec. VI. In the case of ZnSe:Mn (a), no sharp line was observed in a region extending from the zero-phonon lines to the phonon-assisted lines at 19760 cm^{-1}. In the case of ZnS:Mn (b), the lines appearing near 19770 cm^{-1} are due to Mn^{++} in stacking faults.

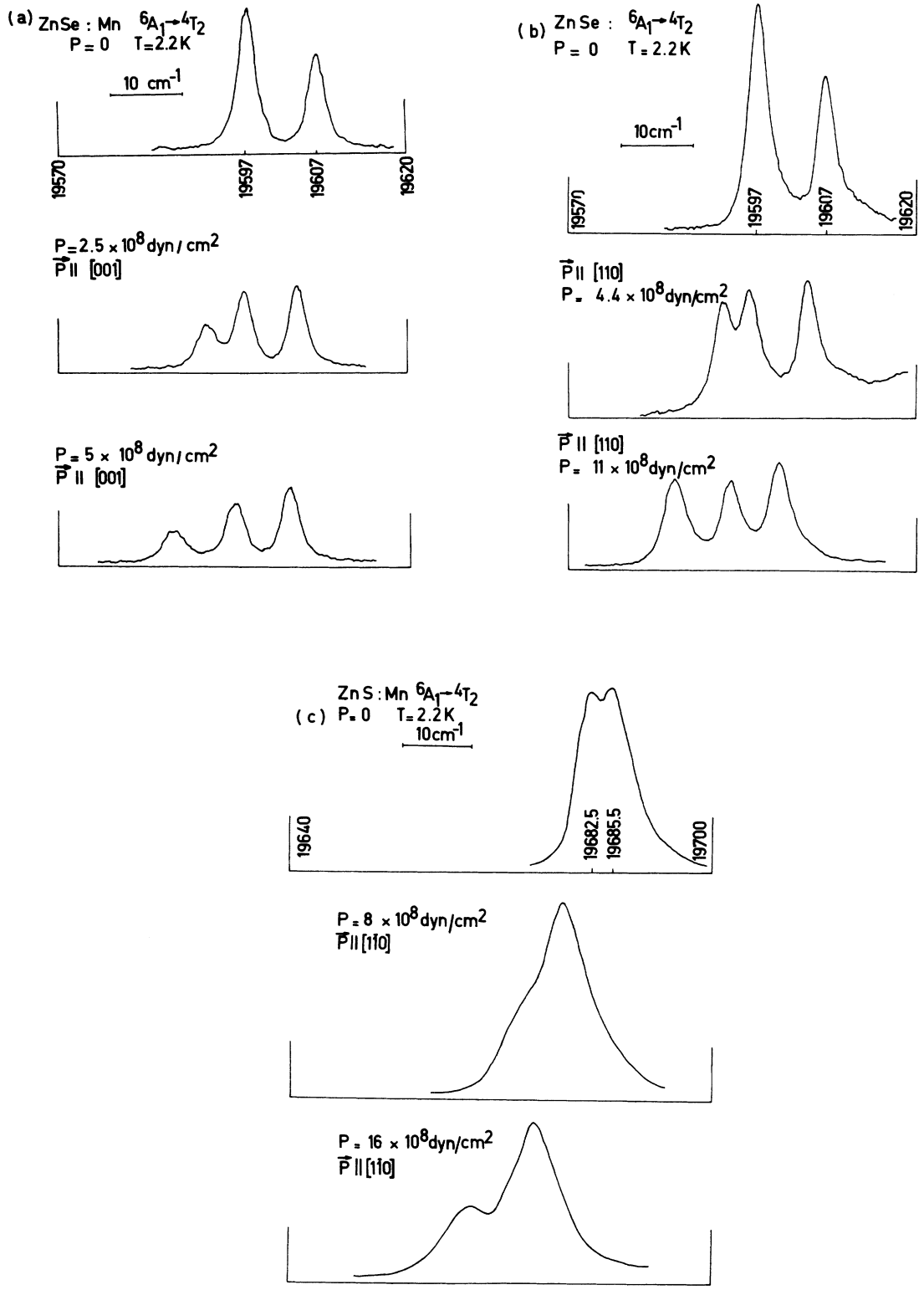

FIG. 3. Influence of uniaxial stresses on the zero-phonon lines reported in Fig. 2. (a) splitting and shifts for ZnSe:Mn, $\vec{P}\|[001]$. (b) ZnSe:Mn $\vec{P}\|[110]$. (c) ZnS:Mn, $\vec{P}\|[1\bar{1}0]$.

in Ref. 10 that the presence of axial sites in our samples does not perturb stress effects on the cubic sites. The dimensions of the crystals were as follows: $8.25 \times 2.85 \times 1.55$ mm^3, the cross-sectional area S perpendicular to the $[1\bar{1}0]$ direction being $S = (2.85 \pm 0.01) \times (1.55 \pm 0.01)$ mm^2; and $5.00 \times 1.25 \times 0.82$ mm^3, S being perpendicular to the $[111]_W$ direction, $S = (1.25 \pm 0.01) \times (0.82 \pm 0.01)$ mm^2.

The stress rig was the same as that used previously.[10,12] The samples were directly immersed in liquid helium. The measurements were performed at 4.2 and sometimes at 2.2 K in order to avoid the bubbling of liquid helium. The spectra remained unchanged when passing from 4.2 to 2.2 K. The measurements were performed with an HRS-2 spectrometer manufactured by Jobin-Yvon. The resolution used in our experiments was 1.5 cm^{-1} at 20 000 cm^{-1}.

B. Experiments

The studied lines are represented in Fig. 2. For ZnSe:Mn, the lines are located at 19 597 and 19 607 cm^{-1}, in agreement with Langer and Richter's results[13] (19 598 and 19 608 cm^{-1}). The lines appearing in the spectra of ZnS:Mn near 19 780 cm^{-1} have been attributed to Mn^{++} ions in stacking faults.[11] Thus the zero-phonon lines of the $^4T_2$ level are those appearing at 19 682.5 and 19 685.5 cm^{-1}, in agreement with Langer and Ibuki's results[9] (19 683 and 19 685.9 cm^{-1}). The interpretation of the very weak line appearing at 19 717 cm^{-1} will be left until later (this line is too weak to give clear results under stress).

For Mn^{++} in ZnSe a shift of all lines and a splitting of the line at lower energy appeared for $\vec{P} \parallel [001]$ and for $\vec{P} \parallel [110]$ even for a relatively low pressure ($P \simeq 3 \times 10^8$ dyn/cm^2) [Figs. 3(a) and 3(b)]. We observed no splitting and no broadening, but we did observe a shift for the line at higher energy. For $\vec{P} \parallel [111]$ no splitting and no measurable broadening was observed.

In the case of Mn^{++} in ZnS, for small values of the applied pressure, $P < 8 \times 10^8$ dyn/cm^2 ($\vec{P} \parallel [110]$), the two lines existing when $P = 0$ are no longer resolved [Fig. 3(c)], (this was not a broadening due to nonuniaxial stresses whose presence or absence was checked by preliminary experiments on the fine-structure lines of the ^4E level). For sufficiently high pressures ($P \geq 8 \times 10^8$ dyn/cm^2), two lines appeared. No splitting and no measurable broadening was observed for $\vec{P} \parallel [111]_W$ even at the higher pressure used ($P = 36 \times 10^8$ dyn/cm^2).

Figure 4 represents the shifts and splittings in terms of the applied pressure. The solid theoretical curves result from the theoretical considerations of the following sections. Figure 5 represents the polarization effects for ZnSe:Mn ($\vec{P} \parallel [001]$ and $\vec{P} \parallel [110]$). The electric field is either perpendicular or parallel to the applied pressure. These experiments show a strong polarization effect for the lines at lower energy.

The experimental results led us to consider first two simple models concerning the structure of the $^4T_2$ level: (i) The level at lower energy, being split by [110] and [100] stresses, could be a pure electronic $\Gamma_8(\frac{5}{2})$ level, the level at higher energy being a Kramer's doublet Γ_6. (ii) The presence of only two lines when $P = 0$ could be explained by Jahn-Teller interactions leading to a strong quenching of the first-order spin-orbit splitting.[14,15] The fact that no measurable splitting appears for $\vec{P} \parallel [111]$ indicates that the $^4T_2$ level is not coupled predominantly to the two T_2 vibrational modes existing in T_d symmetry but rather that it could be coupled to the E vibrational mode. These two models are studied in detail in Secs. III and IV.

III. ASSUMPTION OF PURE ELECTRONIC LEVELS

A. Energy levels in T_d symmetry

For a $^4T_2$ level it can be easily shown that the first-order spin-orbit coupling gives only three distinct electronic levels whose energies are

$$W(\Gamma_6) = W(\Gamma_8(\tfrac{5}{2})) = -(1/2\sqrt{10})R\,,$$

$$W(\Gamma_7) = +(\sqrt{5}/6\sqrt{2})R\,,$$

$$W(\Gamma_8(\tfrac{3}{2})) = +(1/3\sqrt{10})R\,,$$

the energy of the $^4T_2$ level being taken as reference. R is the reduced matrix element of the spin-orbit Hamiltonian $\mathcal{H}_{SO}$ within the $^4T_2$ level. The above energies show that the ratio of the spacings between adjacent levels is simply $\frac{5}{3}$. The mixing parameters α_1', β_1', and γ_1' are defined as

$$|^4T_2\rangle = \alpha_1'|(^4D)T_2\rangle + \beta_1'|(^4F)T_2\rangle + \gamma_1'|(^4G)T_2\rangle\,.$$

R is given by

$$R = (3\sqrt{30}/\sqrt{7})\rho_{3d}\beta_1'\gamma_1' - (8\sqrt{10}/\sqrt{7})\rho_{3d}\alpha_1'\beta_1'\,,$$

ρ_{3d} being the spin-orbit constant for Mn^{++}.

In order to calculate the second-order spin-orbit interaction by taking into account all the relevant multiplets of the $3d^5$ configuration, it is convenient to work in the spinor group T_d^* by making full use of the symmetry properties. First, we can note that the matrix elements intervening in the calculation of the second-order spin-orbit

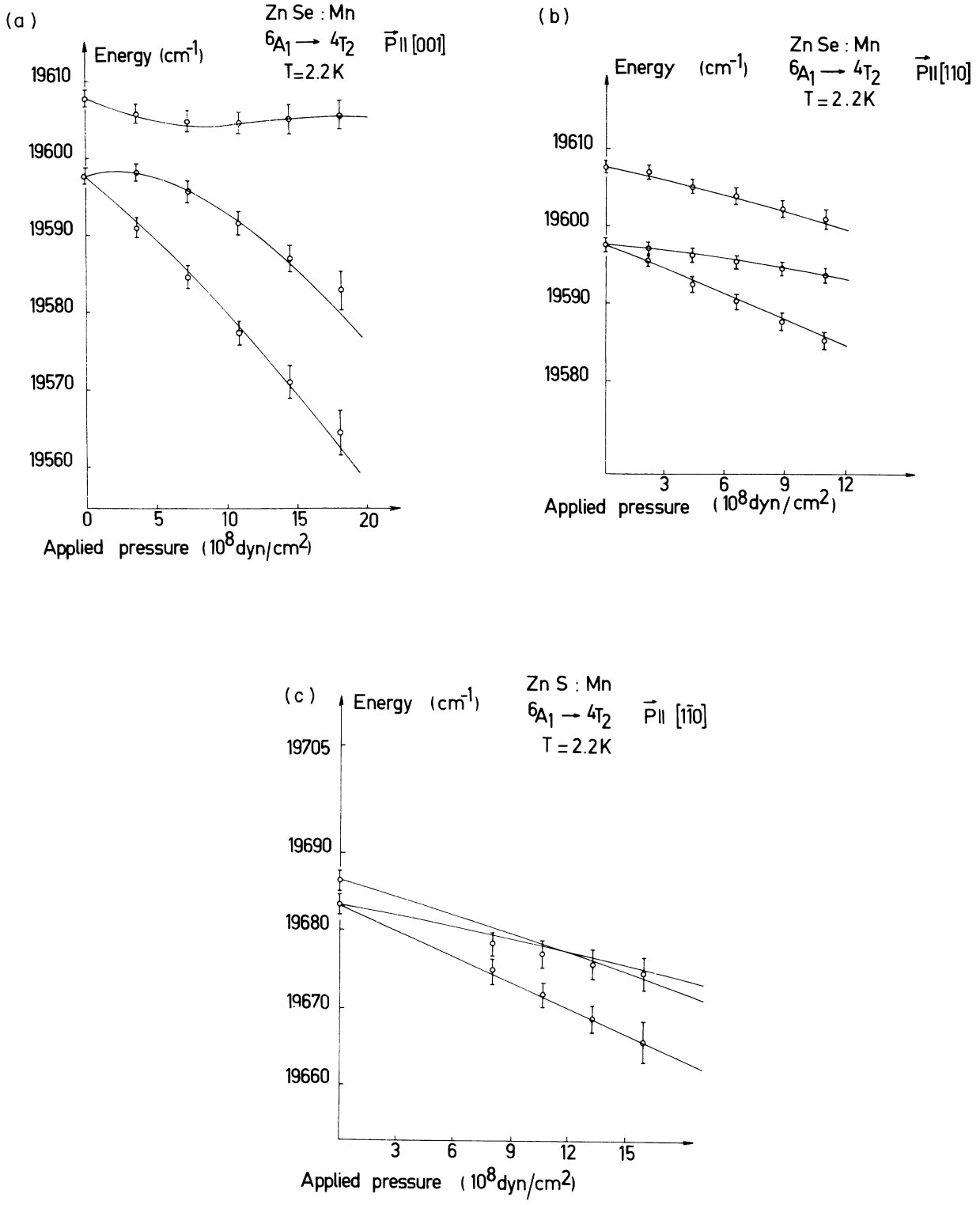

FIG. 4. Splitting and shifts of the zero-phonon lines reported in Fig. 3, in terms of applied pressure. (a) ZnSe:Mn, $\vec{P} \parallel [001]$. (b) ZnSe:Mn, $\vec{P} \parallel [110]$. (c) ZnS:Mn $\vec{P} \parallel [1\bar{1}0]$.

interaction

$$\sum_{S,h,J'} \frac{|\langle(^4T_2)Jt\tau|\mathcal{H}_{SO}|^{2S+1}hJ't\tau\rangle|^2}{W(^4T_2)-W(^{2S+1}h)}$$

are diagonal in $t\tau$ but not in JJ' (the notations are those of Griffith[16]). Then using the Ω of Griffith[16] and defining coefficients $\{^{2S+1}h\}$,

$$\{^{2S+1}h\} = \sum_i \frac{\langle ^4T_2||\mathcal{H}_{SO}||^{2S+1}_i h\rangle\langle ^{2S+1}_i h||\mathcal{H}_{SO}||^4T_2\rangle}{W(^4T_2)-W(^{2S+1}_i h)},$$

we easily obtain the diagonal and nondiagonal matrix elements of the second-order spin-orbit interaction (see Appendix). The complete calculation must be performed by taking into account all 35 relevant multiplets $^4T_1(3)$, $^4T_2(3)$, $^2E(7)$, $^2T_1(8)$, $^2T_2(10)$, $^2A_2(3)$, $^4A_2(1)$ of the $3d^5$ configuration[17] (the number of multiplets of given spin and symmetry are indicated in parentheses), since they all give a non-negligible contribution to the second-order spin-orbit splitting of the $^4T_2$ level considered here.

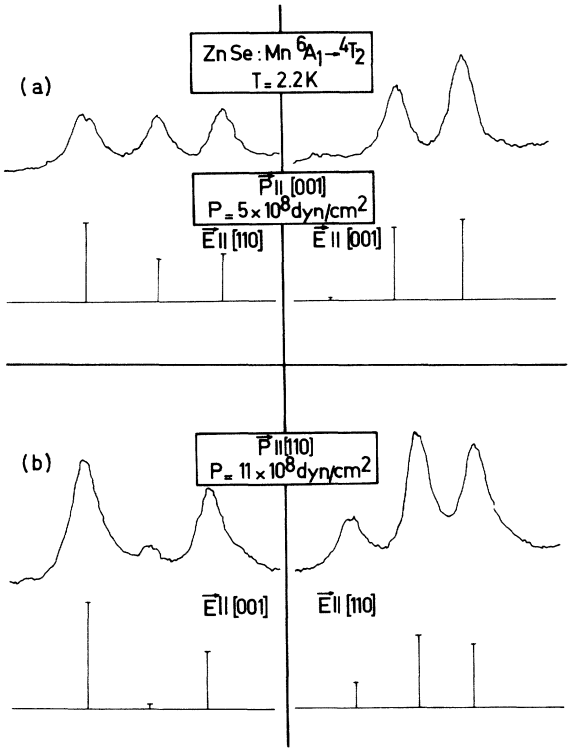

FIG. 5. Polarization effects for (a) $\vec{P}\parallel[001]$ and (b) $\vec{P}\parallel[110]$.

B. Uniaxial-stress effect

For $\vec{P}\parallel[110]$ and $\vec{P}\parallel[100]$, the nonzero linear combinations of the strain tensor are respectively,[12]

$$\epsilon(A_1) = (s_{11}+2s_{12})P, \quad \epsilon(E_u) = -(s_{11}-s_{12})P,$$
$$\epsilon(T_{2\xi}) = \tfrac{1}{2}s_{44}P$$

and

$$\epsilon(A_1) = (s_{11}+2s_{12})P, \quad \epsilon(E_u) = 2(s_{11}-s_{12})P,$$

where the s_{ij} are the elastic-compliance constants of the crystal. A glance at the coupling coefficients in T_d symmetry and the seniority number of the spectroscopic terms intervening in the $^4T_2$ state shows that the degeneracy of the Γ_8 levels can be lifted by the first-order effect of the deformations of E_u and $T_{2\xi}$ symmetry. As usual, the splittings of the Γ_8 levels and the shifts [except those due to $\epsilon(A_1)$] of the Γ_6 and Γ_7 levels will be described by two parameters A and B defined in terms of the variation $\Delta V(E_u)$ and $\Delta V(T_{2\xi})$ of the crystal field in the following manner:

$$A = -\langle ^4T_2|\Delta V(E_u)|^4T_2\rangle,$$
$$B = \langle ^4T_2|\Delta V(T_{2\xi})|^4T_2\rangle.$$

C. Dipole strengths in T_d symmetry

The problem of calculating the dipole strengths for d^n ions has been studied for a long time.[1,18-20] These early works considered mainly the interactions between the d^n and odd-parity configurations via either the internal crystal field or the

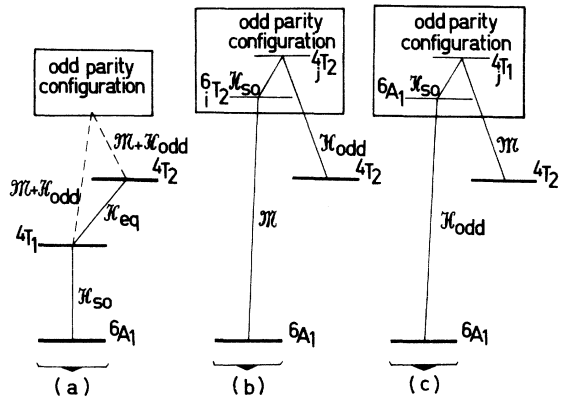

FIG. 6. Schematic representation of the interactions used in the description of the relative dipole strengths of the fine-structure lines of the $^4T_2$ level. Schemes (a), (b), and (c) represent third-order perturbation processes. At this time, no equivalent operator to permit reducing the order of the perturbation in cases (b) and (c) exists.

internal vibrations. Several schemes have been criticized by Griffith,[21] who has remarked in particular that an unrealistic closure theorem was sometimes used and that only one excited configuration was considered. Griffith also gave a method to permit calculating the dipole strengths from symmetry adapted wave functions.[22]

Since the works by Rohrlich using Racah's formalism,[23] more powerful formalisms concerning configuration interactions have been elaborated which include the promotion of an electron from a filled shell to an empty shell or to a half-filled shell and the promotion of an electron from a half-filled shell to an empty shell.[24-27] Thus most of the theoretical inconsistencies or deficiencies recognized by Griffith are now removed.

However, calculating in a rigorous manner all possible contributions to the dipole strengths of a d^5 ion is a formidable task which will not be done here. Rather, we will consider the symmetry properties of various schemes intervening in the interpretation of the dipole strengths and elaborate a parametrization procedure permitting an interpretation of polarization experiments.

Several perturbation schemes can be considered in order to explain the relative dipole strengths of the fine-structure lines of a $^4T_2$ level. Those given in Fig. 6 correspond to the following expression:

$$\mathcal{G}[t(^6A_1) \rightarrow t'(^4T_2)] = \sum_{(^6A_1)\tau} \sum_{(^4T_2)\tau} |A + B + C|^2 ,$$

with

$$A = \sum_{(^4_i T_1) J t\tau} \frac{\langle (^6A_1) t\tau | \mathcal{H}_{SO} | (^4_i T_1) J t\tau \rangle \langle (^4_i T_1) J t\tau | \mathcal{H}_{eq} | (^4T_2) t'\tau' \rangle}{W(^6A_1) - W(^4_i T_1)} ,$$

$$B = \sum_{(^6T_{2odd}) t\tau} \sum_{(^4T_{2odd}) t\tau} \frac{\langle (^6A_1) t\tau | \mathfrak{M} | (^6T_{2odd}) t\tau \rangle \langle (^6T_{2odd}) t\tau | \mathcal{H}_{SO} | (^4T_{2odd}) t\tau \rangle \langle (^4T_{2odd}) t\tau | \mathcal{H}_{odd} | (^4T_2) t'\tau' \rangle}{[W(^4T_2) - W(^6T_{2odd})][W(^4T_2) - W(^4T_{2odd})]} ,$$

$$C = \sum_{(^6A_{1odd}) t\tau} \sum_{(^4T_{1odd}) t\tau} \frac{\langle (^6A_1) t\tau | \mathcal{H}_{odd} | (^6A_{1odd}) t\tau \rangle \langle (^6A_{1odd}) t\tau | \mathcal{H}_{SO} | (^4T_{1odd}) t\tau \rangle \langle (^4T_{1odd}) t\tau | \mathfrak{M} | (^4T_2) t'\tau' \rangle}{[W(^6A_1) - W(^6A_{1odd})][W(^6A_1) - W(^4T_{1odd})]} .$$

The notations are those of Griffith,[21] with $t = \Gamma_7(^6A_1)$, $\Gamma_8(^6A_1)$ and $t' = \Gamma_6(^4T_2)$, $\Gamma_7(^4T_2)$, $\Gamma_8(\frac{3}{2})(^4T_2)$, $\Gamma_8(\frac{5}{2})(^4T_2)$.

The A, B, and C terms correspond to classical interactions relating the fundamental $^6A_1$ level to the $^4T_2$ level. In A, $\mathcal{H}_{eq}$ is an equivalent operator[10] arising from the composition of the electric dipole moment $\vec{\mathfrak{M}}$ with the odd part $\mathcal{H}_{odd}$ of the crystal field and spanning the T_2 representation of the spinor group T_d^*,

$$\mathcal{H}_{eq} = \sum_{\Psi odd} \frac{\mathfrak{M} | \Psi_{odd} \rangle \langle \Psi_{odd} | \mathcal{H}_{odd} + \mathcal{H}_{odd} | \Psi_{odd} \rangle \langle \Psi_{odd} | \mathfrak{M}}{W(3d^5) - W(\Psi_{odd})} .$$

The B and C terms arise from a third-order perturbation via the $^6T_{2odd}$, $^4T_{2odd}$ and $^6A_{1odd}$, $^4T_{1odd}$ states of the excited configurations of odd parity.

These schemes are in fact the simplest contributing to the dipole strengths of the $^4T_2$ level. Other schemes can be elaborated when covalency or relativistic effects are taken into account. However, all schemes linear in $\mathfrak{M}$ have the same symmetry properties.

For example, expressing the terms A, B, and C in terms of three reduced matrix elements, and neglecting the splitting of the $^6A_1$ ground state,[28] we get the following relative dipole strengths:

$$\mathcal{G}[^6A_1 \rightarrow \Gamma_8(\tfrac{5}{2})(^4T_2)] = 14 ,$$

$$\mathcal{G}[^6A_1 \rightarrow \Gamma_6(^4T_2)] = 7 ,$$

$$\mathcal{G}[^6A_1 \rightarrow \Gamma_7(^4T_2)] = 0 ,$$

$$\mathcal{G}[^6A_1 \rightarrow \Gamma_8(\tfrac{3}{2})(^4T_2)] = 9$$

(for $\vec{P} = 0$ and for electric dipolar transitions).

D. Polarization under pressure

The components of the eigenvectors of the matrices describing the pressure effects will be written $(t\tau, J)$ in the following. The relative dipole strengths $\mathcal{G}(\vec{E} \| [100])$, $\mathcal{G}(\vec{E} \| [110])$, and $\mathcal{G}(\vec{E} \| [1\bar{1}0])$ corresponding, respectively, to light polarized along a [100], [110], or [1$\bar{1}$0] crystallographic axis are given by

$$\mathcal{G}(\vec{E}\|[100]) = (1/N^2)[\,|\,(1/3\sqrt{2})(\Gamma_6\tfrac{1}{2}) - (1/\sqrt{10})(\Gamma_8\tfrac{1}{2},\tfrac{3}{2}) - (4/3\sqrt{10})(\Gamma_8\tfrac{1}{2},\tfrac{5}{2})\,|^2 + |\,(3/5\sqrt{2})(\Gamma_8-\tfrac{3}{2},\tfrac{3}{2}) - (1/5\sqrt{2})(\Gamma_8-\tfrac{3}{2},\tfrac{5}{2})\,|^2 + |\,-(2\sqrt{2}/3\sqrt{5})(\Gamma_6\tfrac{1}{2}) + (1/5\sqrt{2})(\Gamma_8\tfrac{1}{2},\tfrac{3}{2}) - (11/15\sqrt{2})(\Gamma_8\tfrac{1}{2},\tfrac{5}{2})\,|^2]$$

and

$$\mathcal{G} = (1/4N^2)\{\,|\,[\tfrac{1}{3}(\Gamma_6\tfrac{1}{2}) + (1/2\sqrt{5})(\Gamma_8\tfrac{1}{2},\tfrac{3}{2}) + (2/3\sqrt{5})(\Gamma_8\tfrac{1}{2},\tfrac{5}{2})](1\pm i) + [(\sqrt{3}/2\sqrt{5})(\Gamma_8-\tfrac{3}{2},\tfrac{3}{2}) + (2/\sqrt{15})(\Gamma_8-\tfrac{3}{2},\tfrac{5}{2})](1\mp i)\,|^2 + |\,[(2/\sqrt{15})(\Gamma_6\tfrac{1}{2}) - (\sqrt{3}/10)(\Gamma_8\tfrac{1}{2},\tfrac{3}{2}) - (2/5\sqrt{3})(\Gamma_8\tfrac{1}{2},\tfrac{5}{2})](1\mp i) + [-\tfrac{3}{10}(\Gamma_8-\tfrac{3}{2},\tfrac{3}{2}) + \tfrac{3}{5}(\Gamma_8-\tfrac{3}{2},\tfrac{5}{2})](1\pm i)\,|^2 + |\,[(2/3\sqrt{5})(\Gamma_6\tfrac{1}{2}) + \tfrac{1}{2}(\Gamma_8\tfrac{1}{2},\tfrac{3}{2}) - \tfrac{1}{3}(\Gamma_8\tfrac{1}{2},\tfrac{5}{2})](1\pm i) + [-(\sqrt{3}/10)(\Gamma_8-\tfrac{3}{2},\tfrac{3}{2}) - (2/5\sqrt{3})(\Gamma_8-\tfrac{3}{2},\tfrac{5}{2})](1\mp i)\,|^2\}\,,$$

where the upper signs correspond to $\mathcal{G}(\vec{E}\|[110])$ and the lower signs to $\mathcal{G}(\vec{E}\|[1\bar{1}0])$. N is a normalization constant.

E. Comparison with experiments

For Mn^{++} in ZnSe, the splitting of the $^4T_2$ electronic level has been calculated from the following values for Racah's parameters and for the cubic field splitting[13]: $B = 740$ cm^{-1}, $C = 2740$ cm^{-1}, and $Dq = -405$ cm^{-1}. Although very tedious, we performed the calculation of the second-order spin-orbit interaction in order to get the order of magnitude for this interaction. The results given in Table I show that the calculated over-all splitting of the $^4T_2$ level is of the order of 120 cm^{-1} and that the second-order spin-orbit coupling shifts all levels by roughly 25 cm^{-1}. More precisely, neglecting the spin-spin interactions,[29] the energy levels are $W(\Gamma_6) = -68.3$ cm^{-1}, $W(\Gamma_7) = +42$ cm^{-1}, $W(\Gamma_8(\frac{3}{2})) = +5.6$ cm^{-1}, and $W(\Gamma_8(\frac{5}{2})) = -62.9$ cm^{-1}, with respect to the $^4T_2$ level. Thus the calculation gives a lower Γ_6 level separated from the $\Gamma_8(\frac{5}{2})$ level by 5.4 cm^{-1}. This result is in contradiction with experiments under stresses which indicate that the lowest level cannot be a Kramer's doublet. Furthermore, this model predicts a relatively strong $^6A_1 \rightarrow \Gamma_8(\frac{3}{2})$ transition which is not observed in experiments, and it must be rejected.

For Mn^{++} in ZnS, the values of the B, C, and Dq parameters are close to those of Mn^{++} in ZnSe ($B = 730$, $C = 2880$, and $Dq = -420$ cm^{-1}),[10] and the results given in this case by the classical model are as bad as for Mn^{++} in ZnSe (see Table I).

IV. DYNAMIC JAHN–TELLER EFFECT: ENERGY LEVELS

A. Weak vibronic interactions

The Hamiltonian governing the vibronic states of a $^4T_2$ electronic state coupled to E vibrational mode is of the form

$$\mathcal{H} = \mathcal{H}_0 + \mathcal{H}_c + \mathcal{H}_{SO} + \mathcal{H}_{el} + \mathcal{H}_K + \mathcal{H}_{JT}\,,$$

where $\mathcal{H}_0$ is the free-ion Hamiltonian, $\mathcal{H}_c$ is the Hamiltonian in a cubic field, $\mathcal{H}_{SO}$ is the spin-orbit Hamiltonian. $\mathcal{H}_{el}$ and $\mathcal{H}_K$ are, respectively, the elastic and kinetic energy associated to the vibra-

TABLE I. First-order and second-order contribution of the spin-orbit interaction to the splitting of the $^4T_2$ level of Mn^{++} in ZnSe and ZnS. Superscripts a and b refer, respectively, to the first-order and second-order contribution of the spin-orbit interaction. The Racah parameters and Dq are given in Sec. III A. The $^4T_2$ level is taken as reference. Spin-orbit parameter: $\rho_{3d} = 300$ cm^{-1}.

	ZnSe			
	Γ_6	Γ_7	$\Gamma_8(\frac{3}{2})$	$\Gamma_8(\frac{5}{2})$
Γ_6	$-46.80^a - 21.50^b$			
Γ_7		$+78.01^a - 35.96^b$		
$\Gamma_8(\frac{3}{2})$			$+31.20^a - 25.62^b$	$+1.80^b$
$\Gamma_8(\frac{5}{2})$			$+1.80^b$	$-46.80^a - 16.11^b$
	ZnS			
Γ_6	$-48.30^a - 21.41^b$			
Γ_7		$+80.49^a - 38.73^b$		
$\Gamma_8(\frac{3}{2})$			$+32.19^a - 19.86^b$	$+1.79^b$
$\Gamma_8(\frac{5}{2})$			$+1.79^b$	$-48.30^a - 15.42^b$

tional mode Q_θ, Q_ϵ belonging to E, explicitly,

$$\mathcal{H}_{e1} = \tfrac{1}{2}\mu\omega(Q_\theta^2 + Q_\epsilon^2)\mathcal{I}, \quad \mathcal{H}_K = (1/2\mu)(P_\theta^2 + P_\epsilon^2)\mathcal{I},$$

the P's being the momentum conjugates to the Q's; $\mathcal{I}$ is the unit matrix, and μ and ω represent, respectively, the effective mass and angular frequency for an effective E mode. $\mathcal{H}_{JT}$ is the interaction Hamiltonian given by

$$\mathcal{H}_{JT} = V(Q_\theta \mathcal{E}_\theta + Q_\epsilon \mathcal{E}_\epsilon),$$

$\mathcal{E}_\theta$ and $\mathcal{E}_\epsilon$ being orbital operators belonging to E. V represents the strength of the Jahn-Teller coupling and is related to the Jahn-Teller energy by $E_{JT} = V^2/2\mu\omega^2$.

In the case of a weak coupling to the E vibrational mode, $\mathcal{H}_{JT}$ is considered as a perturbing Hamiltonian acting between the fundamental vibronic states $|\Gamma_6, 00\rangle$, $|\Gamma_7, 00\rangle$, $|\Gamma_8(\tfrac{3}{2}), 00\rangle$, and $|\Gamma_8(\tfrac{5}{2}), 00\rangle$ and the excited vibronic states with one quantum excited, the vibronic states being products of the electronic states $Jt\tau$ by the wave function for an undisplaced two-dimensional oscillator.[30,31]

The shifts of the energy levels given in Sec. III A are obtained from the following perturbation:

$$\Delta W(Jt\tau) = \sum_{t'\tau' n_\theta n_\epsilon} \frac{(\langle Jt\tau, 00|\mathcal{H}_{JT}|J't'\tau', n_\theta n_\epsilon\rangle)^2}{W(J't') - W(Jt) + \hbar\omega}.$$

Explicitly, we get

$$\Delta W(\Gamma_6) = -\tfrac{1}{30}[W(\Gamma_8(\tfrac{5}{2})) - W(\Gamma_6) + \hbar\omega]^{-1} - \tfrac{3}{10}[W(\Gamma_8(\tfrac{3}{2})) - W(\Gamma_6) + \hbar\omega]^{-1},$$

$$\Delta W(\Gamma_8(\tfrac{5}{2})) = -\tfrac{1}{60}[W(\Gamma_6) - W(\Gamma_8(\tfrac{5}{2})) + \hbar\omega]^{-1} - \tfrac{3}{20}[W(\Gamma_7) - W(\Gamma_8(\tfrac{5}{2})) + \hbar\omega]^{-1} - \tfrac{8}{75}(\hbar\omega)^{-1} - \tfrac{3}{50}[W(\Gamma_8(\tfrac{3}{2})) - W(\Gamma_8(\tfrac{5}{2})) + \hbar\omega]^{-1},$$

$$\Delta W(\Gamma_8(\tfrac{3}{2})) = -\tfrac{3}{20}[W(\Gamma_6) - W(\Gamma_8(\tfrac{3}{2})) + \hbar\omega]^{-1} - \tfrac{1}{60}[W(\Gamma_7) - W(\Gamma_8(\tfrac{3}{2})) + \hbar\omega]^{-1} - \tfrac{3}{50}[W(\Gamma_8(\tfrac{5}{2})) - W(\Gamma_8(\tfrac{3}{2})) + \hbar\omega]^{-1} - \tfrac{8}{75}(\hbar\omega)^{-1},$$

$$\Delta W(\Gamma_7) = -\tfrac{3}{10}[W(\Gamma_8(\tfrac{5}{2})) - W(\Gamma_7) + \hbar\omega]^{-1} - \tfrac{1}{30}[W(\Gamma_8(\tfrac{3}{2})) - W(\Gamma_7) + \hbar\omega]^{-1},$$

in units of $\tfrac{3}{2}V^2\hbar/\mu\omega$.

B. Strong vibronic interactions

We now consider the case of a strong Jahn-Teller interaction between the $^4T_2$ electronic state and the E vibrational mode, that is, $\mathcal{H}_{SO}$ is considered as a perturbing Hamiltonian acting on the vibronic eigenfunctions of the Hamiltonian $\mathcal{H}_0 + \mathcal{H}_c + \mathcal{H}_{e1} + \mathcal{H}_K + \mathcal{H}_{JT}$. We will recall the main results of this well-known problem.

As demonstrated by Ham,[15] the first-order spin-orbit interaction within the fundamental vibronic state is given by the reduced operator

$$\mathcal{H}_{SO}^{(1)} = e^{-3E_{JT}/2\hbar\omega}\mathcal{H}_{SO}.$$

Ham also considered in a very detailed manner the second-order perturbation effects on a vibronic triplet owing to interactions with the vibronic states of the given triplet. Sturge[14] considered second-order perturbation effects connecting different multiplets. When E_{JT} is greater than the spin-orbit splitting of the electronic triplet and when the spacings between the electronic levels involved are greater than E_{JT}, the second-order spin-orbit interactions on a fundamental vibronic triplet $^4T_2$ may be written

$$\langle {}^4T_{2j}, 00|\mathcal{H}_{SO}^2|{}^4T_{2j}, 00\rangle = -\frac{f_b}{\hbar\omega}\sum_{i\neq j}\langle {}^4T_{2j}|\mathcal{H}_{SO}|{}^4T_{2i}\rangle\langle {}^4T_{2i}|\mathcal{H}_{SO}|{}^4T_{2j}\rangle + \sum_{2S+1_h}\frac{\langle {}^4T_{2j}|\mathcal{H}_{SO}|{}^{2S+1}h\rangle\langle {}^{2S+1}h|\mathcal{H}_{SO}|{}^4T_{2j}\rangle}{W({}^4T_2) - W({}^{2S+1}h)}$$

for the diagonal matrix elements. $f_b = e^{-x}G(x)$ with $x = +3E_{JT}/\hbar\omega$ and[15]

$$G(x) = \sum_{n=1}^{\infty}\frac{x^n}{n(n!)}.$$

In the second term, the summation must be performed on all of the relevant multiplets ^{2S+1}h connected by $\mathcal{H}_{SO}$ to the $^4T_{2j}$ triplet.

For the off-diagonal matrix elements we obtain

$$\langle {}^4T_{2j}, 00|\mathcal{H}_{SO}^2|{}^4T_{2k}, 00\rangle = -(f_a/\hbar\omega)\langle {}^4T_{2j}|\mathcal{H}_{SO}|{}^4T_{2i}\rangle\langle {}^4T_{2i}|\mathcal{H}_{SO}|{}^4T_{2k}\rangle + e^{-x/2}\sum_{2S+1_h}\frac{\langle {}^4T_{2j}|\mathcal{H}_{SO}|{}^{2S+1}h\rangle\langle {}^{2S+1}h|\mathcal{H}_{SO}|{}^4T_{2k}\rangle}{W({}^4T_2) - W({}^{2S+1}h)},$$

with $f_a = e^{-x} G(\frac{1}{2}x)$.

Given the number of multiplets intervening in the calculation of the second-order spin-orbit interaction for a $^4T_2$ level of Mn^{++}, we did not use the method of equivalent operators. Instead, we used the fact that the matrix elements of $\mathcal{H}_{SO}^2$ are known in the $^{2S+1}hJt\tau$ scheme. First, the matrix elements of $\mathcal{H}_{SO}^2$ are written in the real tetragonal system $^{2S+1}hM\theta$; we then take the diagonal matrix elements in this scheme and, finally, we calculate these diagonal elements in the $^{2S+1}hJt\tau$ scheme. Thus the contribution of the diagonal (in the real $^{2S+1}hM\theta$ scheme) matrix elements to $\mathcal{H}_{SO}^2$ are given in terms of the matrix elements of $\mathcal{H}_{SO}^2$ in the $^4T_2 Jt\tau$ scheme (see Appendix).

The contribution of the off-diagonal matrix elements is

$$\langle t\tau J|\mathcal{H}_{SO}^2|t\tau J'\rangle_{\text{off-diag}} = \langle t\tau J|\mathcal{H}_{SO}^2|t\tau J'\rangle - \langle t\tau J|\mathcal{H}_{SO}^2|t\tau J'\rangle_{\text{diag}}.$$

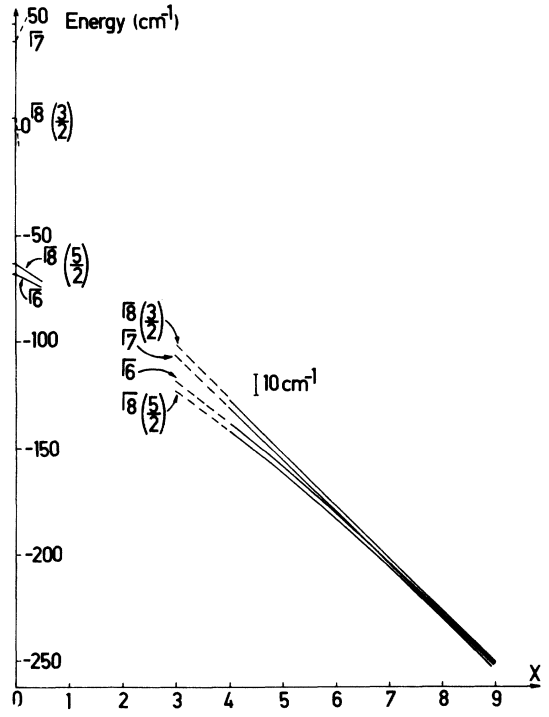

FIG. 7. Influence of weak, medium, and strong vibronic interactions. Case of a coupling to an E vibrational mode. The energy levels are given in terms of $x = 3V^2/2\mu\hbar\omega^3$ for weak interactions and $x = 3E_{JT}/\hbar\omega$ for strong interactions. The solid curves were obtained from a perturbation method. The dashed curves are drawn approximately in the region where the perturbation method is no longer valid in order to get an idea of the shifts before doing a diagonalization of the vibronic Hamiltonian. The parameter R (defined in Sec. III A) is 295 cm^{-1}. $\hbar\omega = 75$ cm^{-1}.

This method permitted us to determine in a simple way the contributions to $\mathcal{H}_{SO}^2$ of the diagonal and off-diagonal matrix elements arising from all multiplets connected to the $^4T_2$ level (see Appendix).

C. Comparison with experiments

Although we performed calculations where the energy of the effective E-mode phonon was successively chosen to be 240, 220, and 75 cm^{-1} from phonon density of states, phonon frequencies and symmetries obtained by Hennion *et al.*[32] from neutron inelastic scattering experiments, we will present, for conciseness only, the results obtained with an effective phonon energy of $\hbar\omega = 75$ cm^{-1} (anticipating the results of Sec. VI, this will be the value finally adopted to account for all experimental results). The parameter R describing the first-order spin-orbit coupling is simply chosen to be $R = 295$ cm^{-1} as given by the crude crystal-field model of Sec. III A.

In the case of weak and strong Jahn-Teller interactions, the energy levels are given, respectively, in terms of $x = 3V^2/2\mu\hbar\omega^3$ and $x = 3E_{JT}/\hbar\omega$ in Fig. 7. In the case of strong Jahn-Teller interactions, the conditions for validity of the perturbation treatment are verified for $x > 3$. When Ham's effect is restricted to the studied level, the splitting of the two lowest levels decreases monotonically from 7 to 3 cm^{-1} when x increases from 3 to 9, the $|\Gamma_8(\frac{5}{2})00\rangle$ level being the lowest. The contribution to this splitting of the second-order spin-orbit interactions with all other relevant multiplets of the d^5 configuration is less than 2 cm^{-1} for $3 < x < 9$.

The most important result appearing in Fig. 7 is that strong vibronic interactions corresponding to $x \sim 4$ could explain the presence of only two absorption lines separated by 10 cm^{-1}. Unfortunately, the results of the uniaxial-stress experiments will lead us to reject this hypothesis. In fact, in the case of a strong Jahn-Teller effect, the two observed lines in T_d symmetry correspond to the almost degenerate $|\Gamma_7, 00\rangle$ and $|\Gamma_8(\frac{3}{2}), 00\rangle$ levels for the line at higher energy and to the almost degenerate $|\Gamma_6, 00\rangle$ and $|\Gamma_8(\frac{5}{2}), 00\rangle$ levels for the other line. Therefore, neglecting any small splitting of the $|\Gamma_7, 00\rangle$ and $|\Gamma_8(\frac{3}{2}), 00\rangle$ levels as well as any splitting of the $|\Gamma_6, 00\rangle$ and $|\Gamma_8(\frac{5}{2}), 00\rangle$ levels when $\vec{P} = 0$, we obtain the energy levels in terms of the A parameter for Mn^{++} in ZnSe as represented in Fig. 8 (see also Table II A). A comparison with the experimental splitting given in Fig. 4 shows that this model cannot describe correctly the stress effect. Furthermore, given the strong mixing of all vibronic levels under an applied pres-

sure $\vec{P}\|[110]$ or $\vec{P}\|[001]$, at least four lines should be observed when $\vec{P}\neq 0$.

To summarize, we have shown that neither the hypothesis of pure electronic levels nor the hypothesis of a weak or strong Jahn-Teller coupling to E vibrational mode give a satisfactory interpretation of the experimental results. Therefore these preliminary studies led us to carefully consider the influence of medium Jahn-Teller interactions on the energy levels and on the dipole strengths. In order to avoid the limitations of a perturbation method, we calculated the wave functions of the fundamental and excited vibronic levels by diagonalizing the vibronic Hamiltonian. The results of this calculation are given in Secs. V and VI.

V. DYNAMIC JAHN TELLER EFFECT: INTENSITY TRANSFER

The diagonalization of the Hamiltonian $\mathcal{H}_{SO}+\mathcal{H}_{el}+\mathcal{H}_K+\mathcal{H}_{JT}$ defined in Sec. IV A was performed for one $^4T_2$ state. All interactions between the $^4T_2$ state and others multiplets of the d^5 configuration were neglected; in particular, our results will not reflect the spin-orbit interactions with other multiplets as it was the case in Sec. IV.

The matrix elements of $\mathcal{H}_{SO}$, $\mathcal{E}_\theta$, and $\mathcal{E}_\epsilon$ were calculated in T_d^*. The dimension of the matrices were $3(n'+1)(n'+2)$, n' being the number of phonons introduced in the calculation. The diagonalizations were performed with either three or five phonons, the choice of the number of phonons being governed by the convergency of the mixing

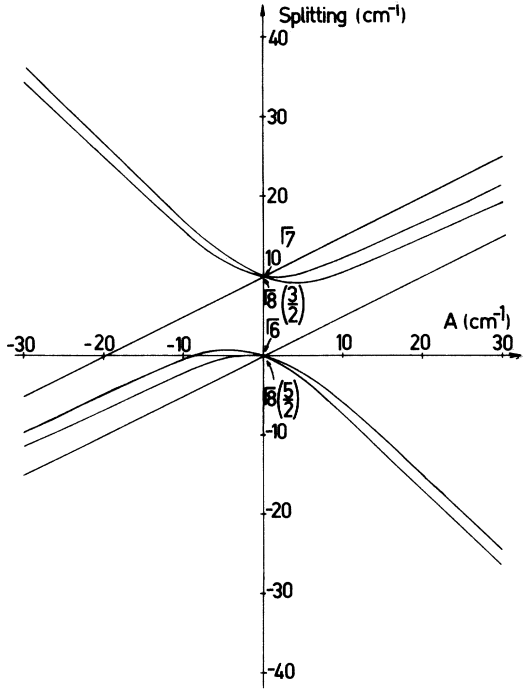

FIG. 8. Theoretical splitting of the $^4T_2$ level of Mn^{++} in ZnSe in terms of A, in the case of a strong coupling to an E vibrational mode. The parameter A is defined in Sec. III B.

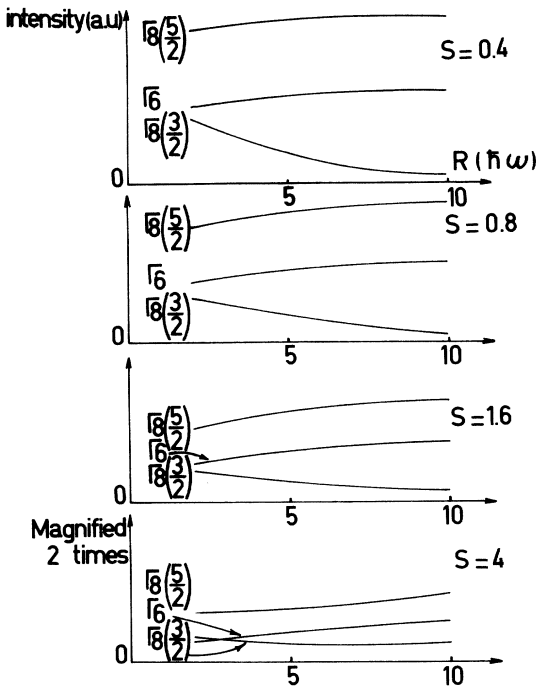

FIG. 9. Relative dipole strengths of the zero-phonon lines for a $^4T_2$ state in terms of R, for different values of S (R is defined in Sec. III A and S in Sec. V). The indexation of the zero-phonon lines is that of pure electronic levels obtained by continuity when $S\to 0$.

TABLE II. Matrix elements of the pressure-induced crystal field for $\vec{P}\|[100]$. A is defined in Sec. III B. The $\alpha(tJ)$ are the diagonal matrix elements when $\vec{P}=0$ (owing to the first-order and second-order spin-orbit interactions). β is the nondiagonal term owing to the second-order spin-orbit interaction. The shift common to all levels owing to the variation of Dq is omitted.

	$\Gamma_6\pm\frac{1}{2}$	$\Gamma_8(\frac{3}{2})\pm\frac{1}{2}$	$\Gamma_8(\frac{5}{2})\pm\frac{1}{2}$
$\Gamma_6\pm\frac{1}{2}$	$\alpha(\Gamma_6)$	$\mp(3/2\sqrt{5})$	$\pm(1/2\sqrt{5})A$
$\Gamma_8(\frac{3}{2})\pm\frac{1}{2}$		$\alpha[\Gamma_8(\frac{3}{2})]-\frac{2}{5}A$	$+\frac{3}{10}A+\beta$
$\Gamma_8(\frac{5}{2})\pm\frac{1}{2}$			$\alpha[\Gamma_8(\frac{5}{2})]+\frac{2}{5}A$
	$\Gamma_7\pm\frac{1}{2}$	$\Gamma_8(\frac{3}{2})\mp\frac{3}{2}$	$\Gamma_8(\frac{5}{2})\mp\frac{3}{2}$
$\Gamma_7\pm\frac{1}{2}$	$\alpha(\Gamma_7)$	$\mp(1/2\sqrt{5})A$	$\mp(3/2\sqrt{5})A$
$\Gamma_8(\frac{3}{2})\mp\frac{3}{2}$		$\alpha[\Gamma_8(\frac{3}{2})]+\frac{2}{5}A$	$-\frac{3}{10}A+\beta$
$\Gamma_8(\frac{5}{2})\mp\frac{3}{2}$			$\alpha[\Gamma_8(\frac{5}{2})]-\frac{2}{5}A$

parameters ($^4T_2$, $t\tau J$, n, $n_\theta n_\epsilon$) of the vibronic wave functions

$$|^4T_2, n\rangle = \sum_{t,\tau,J,n_\theta n_\epsilon} (^4T_2, t\tau J, n, n_\theta n_\epsilon)\,|^4T_2, t\tau J, n_\theta n_\epsilon\rangle ,$$

where n refers to the nth vibronic level.

Before giving the results concerning the intensity transfer in a $^4T_2$ state, we must remark that the products of matrix elements intervening in the formulas giving the relative dipole strengths (Secs. III C and III D) may be simply multiplied by the mixing parameters ($^4T_2, t\tau J, n, 00$) when we are concerned either by the zero-phonon levels of the $^4T_2$ state or by the phonon-assisted levels of this state. Of course, this simple procedure is valid only when the spacings between the electronic levels involved are greater than the Jahn-Teller energy associated with these levels. In particular, we will use directly the formulas given in Sec. III D by replacing the ($t\tau, J$) by the ($^4T_2, t\tau J, n, 00$).

Figure 9 shows the calculated relative dipole strengths in terms of the parameter $R/\hbar\omega$ measuring the spin-orbit splittings of the $^4T_2$ state (R is defined in Sec. III A) for different values of the Huang-Rhys factor $S = E_{JT}/\hbar\omega$. This figure shows that for a given S the dipole strengths of the $^6A_1 \rightarrow \Gamma_6$ and $^6A_1 \rightarrow \Gamma_8(\frac{5}{2})$ zero-phonon lines remain almost constant for increasing values of R while the dipole strength of the $^6A_1 \rightarrow \Gamma_8(\frac{3}{2})$ line

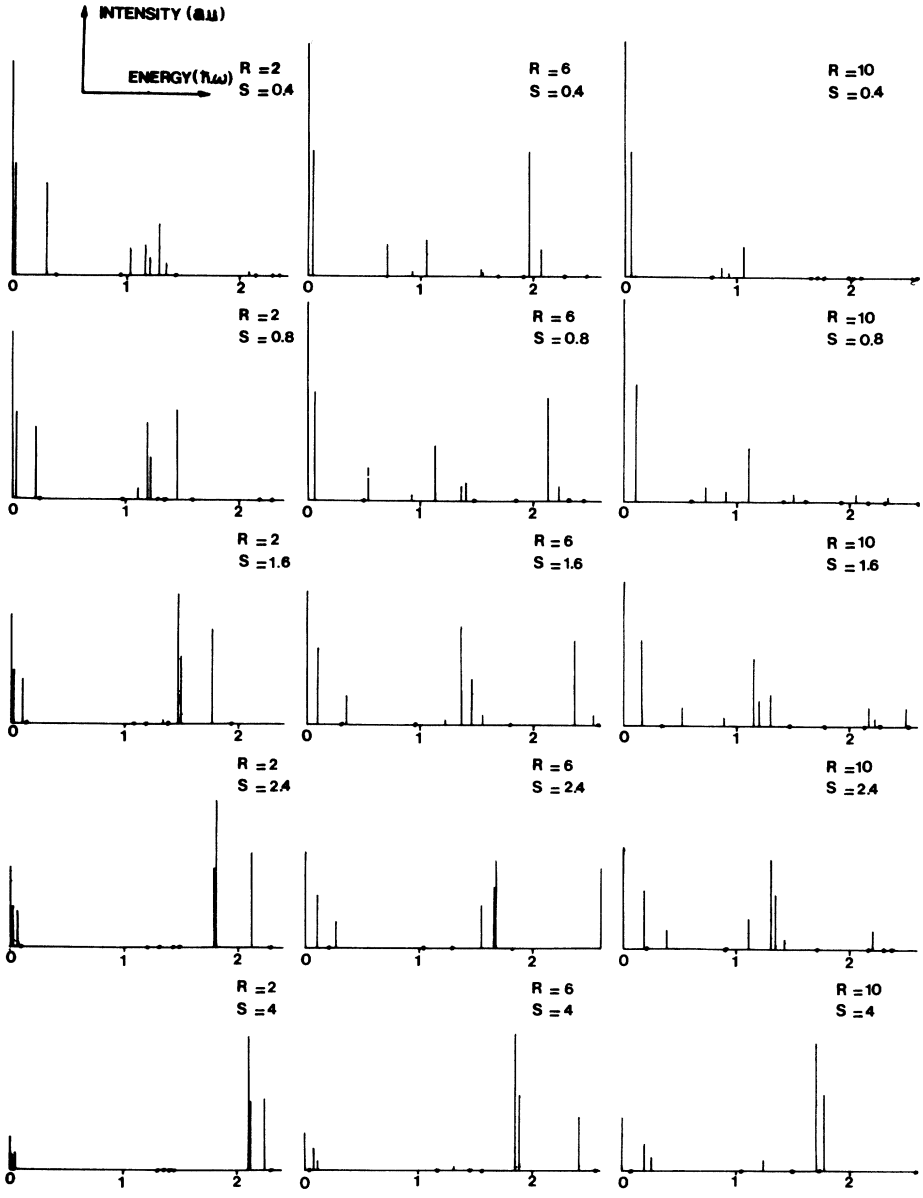

FIG. 10. Energy levels and intensity of the zero-phonon lines and phonon-assisted lines for a $^4T_2$ state. Points indicate zero or negligible dipole strengths. R is given in units of $\hbar\omega$.

decreases monotonically for increasing values of R. On the other hand, this figure shows that for a given R the dipole strengths of the zero-phonon lines decrease monotonically from the values 14, 7, and 9 (for $S=0$) to the almost proportional values of 1.5, 0.7, and 0.8 (for $S=4$ and $R/\hbar\omega=2$) when strong vibronic interactions occur.

In order to get a deeper insight of the mechanism leading to the intensity transfer, we show in Fig. 10 the positions and the relative dipole strengths of the zero-phonon lines and one-phonon-assisted lines for different values of $R/\hbar\omega$ and S. In Fig. 10 we do not try to give an indexing for the phonon-assisted lines since they depend on too many mixing parameters having the same order of magnitude.

VI. STRUCTURE OF THE LOWEST $^4T_2$ LEVEL FOR Mn^{++} IN ZnSe AND ZnS

By using the results of Sec. V as a guide, we have elaborated a coherent model to interpret all experimental results reported in Sec. II B.

The experimental results to be fitted were the energy levels and dipole strengths for the zero-pressure spectra and for the pressure-induced spectra and the dipole strengths for polarized light. The main parameters intervening in our model were the Huang-Rhys factor S and the parameter R describing the first-order spin-orbit splitting of the $^4T_2$ level. Although the crystal-field model permits us to calculate R (Sec. III A), we considered it as a parameter to be fitted to experiments for the following reasons: First, we cannot verify the correctness of the calculated value for R since the first-order spin-orbit splitting of the $^4T_2$ level cannot be deduced from the observed spectra; second, it is impossible to account for the experimental results in the case of ZnSe when using the value for R as given by the crystal-field model, thus indicating that covalency can be of importance when Se ligands are involved.

In the case of ZnSe:Mn, we used an effective E-mode phonon of energy $\hbar\omega=75$ cm^{-1}; this value is close to that of 69 cm^{-1} chosen by Vallin and Watkins[33] in interpreting the EPR spectra for Cr^{2+} ions in ZnSe and identical to the value chosen by Nygren *et al.*[34] in interpreting infrared absorption for ZnSe:Cr. All our experimental results were correctly fitted by $S=1.2$ and $R/\hbar\omega=10$ (this last value is 2.5 times larger than that given by the crystal-field model of Sec. III A). The theoretical energy levels and dipole strengths for $\vec{P}=0$ are compared with experiments in Fig. 2(a). This figure shows clearly the very good agreement between theory and experiment for the two observed lines; it also demonstrates the importance of intensity transfer for the $^6A_1 \rightarrow \Gamma_8(\frac{3}{2})$ line [the point in Fig. 2(a) represents the forbidden $^6A_1 \rightarrow \Gamma_7$ transition].

The pressure effects reported in Figs. 4(a) and 4(b) were correctly fitted by taking $A=3650$ cm^{-1} per unit strain. The shift common to all lines is 11 500 cm^{-1} per unit strain. The needed elastic compliance constants were measured at 25 °C by Berlincourt *et al.*[35]: $s_{11}=2.26\times10^{-12}$ cm^2/dyn and $s_{12}=-0.85\times10^{-12}$ cm^2/dyn.

The theoretical line positions and relative dipole strengths given in Fig. 5 (see also Table III) were obtained by diagonalizing the vibronic and pressure-induced Hamiltonian using the above values of S, R, and A. We must note the excellent agreement between theory and experiments in all considered cases.

Finally, we have checked in another way the validity of the cluster model used in our calculations by estimating S from the pressure effects. In tetrahedral coordination S is given by[36]

$$S=(1/2\mu\hbar\omega^3)(6A/2\sqrt{2}R)^2,$$

where μ is the effective mass of the E mode and R is the nearest-neighbor distance. In our case we obtained $S=5.0$, in rough agreement with the value chosen in our calculations ($S=1.2$).

In the case of ZnS:Mn, we used an effective E mode phonon of energy $\hbar\omega=100$ cm^{-1}. This energy is in agreement with that chosen by Vallin and Watkins[33] in analyzing the EPR spectra of ZnS:Cr; it is also the energy of the low-frequency mode chosen by Ham and Slack[31] in interpreting the optical spectra of Fe^{++} in ZnS. By taking $S=0.6$ and $R/\hbar\omega=3.5$ (this last value is in correct agreement with the value 3 given by the crystal-field

TABLE III. Theoretical relative dipole strengths for $\vec{P}\parallel[100]$ and $\vec{P}\parallel[110]$ in the case of Mn^{++} in ZnSe. The theoretical and experimental results are compared in Fig. 5.

$\vec{P}\parallel[001]$ ($P=5\times10^8$ dyn/cm^2)	Line at higher energy	Central line	Line at lower energy
Dipole strengths			
$\vec{E}\parallel[001]$	6.88	6.21	0.28
$\vec{E}\parallel[110]$	4.06	3.66	6.75
$\vec{P}\parallel[110]$ ($P=1.1\times10^7$ dyn/cm^2)			
Dipole strengths			
$\vec{E}\parallel[001]$	4.95	0.35	9.28
$\vec{E}\parallel[110]$	5.17	6.25	2.09

model), we get the following energies with respect to the $\Gamma_8(\frac{5}{2})$ level:

$$W(\Gamma_6) = 3.3 \text{ cm}^{-1} \text{ (experiment, 3 cm}^{-1}),$$

$$W(\Gamma_8(\tfrac{3}{2})) = 40 \text{ cm}^{-1},$$

and

$$W(\Gamma_7) = 45 \text{ cm}^{-1}.$$

This model led us to tentatively associate the small absorption line appearing at 19 917 cm^{-1} to the $^6A_1 \rightarrow \Gamma_8(\frac{3}{2})$ transition (this line is observed in cubic ZnS,[11] and cannot be an absorption line of Mn^{++} ions in stacking faults). The calculated positions and relative dipole strengths for $\vec{P} = 0$ are given in Fig. 2(b). The agreement between theory and experiment is not as good as for ZnSe:Mn; however, we must remark that the presence of stacking faults in our samples perturbs the intensity of the two lines at lower energy and, in particular, the intensity of the line at 19 685.5 cm^{-1} is smaller than the intensity of the line at 19 682.5 cm^{-1} in cubic ZnS.[11] (Unfortunately, the cubic ZnS:Mn crystals at our disposal were too small to be cut and polished in order to perform uniaxial-stress experiments.)

The pressure-induced splittings and shifts given in Fig. 4(c) were fitted with $A = 3100$ cm^{-1} per unit strain, the shift of all lines being 18 000 cm^{-1} per unit strain ($s_{11} = 1.786 \times 10^{-12}$, $s_{12} = 0.685 \times 10^{-12}$ cm^2/dyn at 77 K).[35] The estimation of S from the pressure effects gives $S = 4$, in rough agreement with the chosen value ($S = 0.6$).

VII. CONCLUSION

The structure of a $^4T_2$ level of a d^5 ion in T_d symmetry has been analyzed first in a classical model in which vibronic interactions are neglected. Convenient formulas permitting the calculation of second-order spin-orbit interactions and relative dipole strengths have been reviewed. It has been shown that this model fails to give the correct relative dipole strengths in the case of Mn^{++} in ZnSe and ZnS.

In a second model we have described in a detailed manner the influence of a coupling to E vibrational modes by extending the calculation of the second-order spin-orbit interactions to the d^5 configuration. Ham's and Sturge's perturbation methods were used for that purpose. This model was considered because the existence of strong Jahn-Teller interactions could have explained simply the presence of only two absorption lines observed in experiments ($P = 0$). However, this assumption of strong Jahn-Teller interactions was found to be in disagreement with experimental pressure effects.

Then, by diagonalizing the vibronic Hamiltonian, we have given a general description of the influence of the Jahn-Teller interaction on the energy levels of the zero-phonon and phonon-assisted lines, and on the intensity transfer in a $^4T_2$ level. Coherent values for the Huang-Rhys factors and for the effective phonon energies permitted us to interpret correctly all experiments performed on the lowest $^4T_2$ level of Mn^{++} in ZnSe and ZnS.

Finally, we must emphasize the fact that the classical model often used until now in interpreting the optical spectra of d^5 ions in solids must be handled with caution, particularly when low-energy phonons are observed in the absorption spectra.

ACKNOWLEDGMENTS

Thanks are due to Dr. B. Clerjaud, Dr. A. Gelineau and Dr. C. Blanchard for very helpful discussions concerning Jahn-Teller interactions and to Dr. R. Romestain for giving us the ZnSe:Mn samples used in this work. One of us (R. P.) acknowledges Professor D. S. McClure for a discussion on the structure of triply degenerate states of Mn^{++}. We are indebted to N. Machorine, G. Vandenborghe, and P. Villermet for cutting and polishing several samples used in our experiments.

APPENDIX

Matrix elements of the second-order spin-orbit interactions in the case of strong or medium Jahn-Teller effects are dealt with here. The notations are defined in Secs. III A and IV. The matrix elements for pure electronic levels are obtained by nulling R and x:

$$\langle (^4T_2)\Gamma_6 | \mathcal{H}_{SO}^2 | (^4T_2)\Gamma_6 \rangle = -\left(\tfrac{1}{60} f_b + \tfrac{1}{120} f_a\right) R^2/\hbar\omega + \tfrac{1}{20}\left(-1 + e^{-x/2}\right)\{^4A_2\} + \tfrac{1}{24}\left(-1 + e^{-x/2}\right)\{^2T_2\} + \tfrac{1}{24}\left(1 + e^{-x/2}\right)\{^2T_1\}$$
$$+ \left(\tfrac{1}{20} + \tfrac{1}{40} e^{-x/2}\right)\{^4E\} + \left(-\tfrac{1}{60} + \tfrac{1}{120} e^{-x/2}\right)\{^4T_1\} + \left(\tfrac{1}{60} + \tfrac{1}{120} e^{-x/2}\right)\{^4T_2\},$$

$$\langle (^4T_2)\Gamma_7 | \mathcal{H}_{SO}^2 | (^4T_2)\Gamma_7 \rangle = -\left(\tfrac{7}{180} f_b + \tfrac{11}{360} f_a\right) R^2/\hbar\omega + \left(\tfrac{1}{18} + \tfrac{1}{9} e^{-x/2}\right)\{^2A_2\} + \tfrac{1}{180}\left(-1 + e^{-x/2}\right)\{^4A_2\} - \tfrac{1}{72}\left(1 + e^{-x/2}\right)\{^2T_2\}$$
$$+ \tfrac{1}{18}\left(-1 + e^{-x/2}\right)\{^2E\} + \tfrac{1}{72}\left(1 - e^{-x/2}\right)\{^2T_1\} + \left(\tfrac{1}{180} + \tfrac{1}{360} e^{-x/2}\right)\{^4E\} + \left(-\tfrac{7}{180} + \tfrac{11}{360} e^{-x/2}\right)\{^4T_1\}$$
$$+ \left(\tfrac{7}{180} + \tfrac{11}{360} e^{-x/2}\right)\{^4T_2\},$$

$$\langle(^4T_2)\Gamma_8(\tfrac{3}{2})\,|\,\mathcal{H}^2_{SO}\,|\,(^4T_2)\Gamma_8(\tfrac{3}{2})\rangle = -(\tfrac{17}{900}f_b - \tfrac{7}{900}f_a)R^2/\hbar\omega + \tfrac{1}{180}(1-e^{-x/2})\{^2A_2\} - (\tfrac{41}{900}+\tfrac{34}{900}e^{-x/2})\{^4A_2\} - (\tfrac{7}{180}+\tfrac{11}{360}e^{-x/2})\{^2T_2\}$$
$$-(\tfrac{1}{180}+\tfrac{1}{360}e^{-x/2})\{^2E\} + (\tfrac{7}{180}-\tfrac{11}{360}e^{-x/2})\{^2T_1\} + (\tfrac{41}{900}-\tfrac{17}{900}e^{-x/2})\{^4E\}$$
$$-(\tfrac{17}{900}+\tfrac{7}{900}e^{-x/2})\{^4T_1\} + (\tfrac{17}{900}-\tfrac{7}{900}e^{-x/2})\{^4T_2\},$$

$$\langle(^4T_2)\Gamma_8(\tfrac{5}{2})\,|\,\mathcal{H}^2_{SO}\,|\,(^4T_2)\Gamma_8(\tfrac{5}{2})\rangle = -(\tfrac{11}{300}f_b - \tfrac{7}{600}f_a)R^2/\hbar\omega + \tfrac{1}{20}(1-e^{-x/2})\{^2A_2\} + \tfrac{1}{100}(-1+e^{-x/2})\{^4A_2\}$$
$$+\tfrac{1}{60}(-1+e^{-x/2})\{^2T_2\} - (\tfrac{1}{20}+\tfrac{1}{40}e^{-x/2})\{^2E\} + \tfrac{1}{60}(1+e^{-x/2})\{^2T_1\} + (\tfrac{1}{100}+\tfrac{1}{200}e^{-x/2})\{^4E\}$$
$$-(\tfrac{11}{300}+\tfrac{7}{600}e^{-x/2})\{^4T_1\} + (\tfrac{11}{300}-\tfrac{7}{600}e^{-x/2})\{^4T_2\},$$

$$\langle(^4T_2)\Gamma_8(\tfrac{3}{2})\,|\,\mathcal{H}^2_{SO}\,|\,(^4T_2)\Gamma_8(\tfrac{5}{2})\rangle = -\tfrac{1}{150}(f_b - f_a)R^2/\hbar\omega + \tfrac{1}{60}(1-e^{-x/2})\{^2A_2\} + \tfrac{4}{300}(1-e^{-x/2})\{^4A_2\} + \tfrac{1}{120}(1-e^{-x/2})\{^2T_2\}$$
$$-(\tfrac{1}{60}+\tfrac{1}{120}e^{-x/2})\{^2E\} - \tfrac{1}{120}(1+e^{-x/2})\{^2T_1\} - (\tfrac{1}{150}+\tfrac{1}{75}e^{-x/2})\{^4E\}$$
$$-\tfrac{1}{150}(1+e^{-x/2})\{^4T_1\} + \tfrac{1}{150}(1-e^{-x/2})\{^4T_2\}.$$

The contribution to $\mathcal{H}^2_{SO}$ of the diagonal and off-diagonal matrix elements in the real $^{2S+1}hM\theta$ scheme were calculated in terms of the classical matrix elements of $\mathcal{H}^2_{SO}$ by the following relations:

$$\langle\Gamma_6\,|\,\mathcal{H}^2_{SO}\,|\,\Gamma_6\rangle_{diag} = \tfrac{1}{3}\langle\Gamma_6\,|\,\mathcal{H}^2_{SO}\,|\,\Gamma_6\rangle + \tfrac{3}{5}\langle\Gamma_8(\tfrac{3}{2})\,|\,\mathcal{H}^2_{SO}\,|\,\Gamma_8(\tfrac{3}{2})\rangle + \tfrac{1}{15}\langle\Gamma_8(\tfrac{5}{2})\,|\,\mathcal{H}^2_{SO}\,|\,\Gamma_8(\tfrac{5}{2})\rangle - \tfrac{2}{5}\langle\Gamma_8(\tfrac{3}{2})\,|\,\mathcal{H}^2_{SO}\,|\,\Gamma_8(\tfrac{5}{2})\rangle,$$

$$\langle\Gamma_7\,|\,\mathcal{H}^2_{SO}\,|\,\Gamma_7\rangle_{diag} = \tfrac{1}{3}\langle\Gamma_7\,|\,\mathcal{H}^2_{SO}\,|\,\Gamma_7\rangle + \tfrac{1}{15}\langle\Gamma_8(\tfrac{3}{2})\,|\,\mathcal{H}^2_{SO}\,|\,\Gamma_8(\tfrac{3}{2})\rangle + \tfrac{3}{5}\langle\Gamma_8(\tfrac{5}{2})\,|\,\mathcal{H}^2_{SO}\,|\,\Gamma_8(\tfrac{5}{2})\rangle + \tfrac{2}{5}\langle\Gamma_8(\tfrac{3}{2})\,|\,\mathcal{H}^2_{SO}\,|\,\Gamma_8(\tfrac{5}{2})\rangle,$$

$$\langle\Gamma_8(\tfrac{3}{2})\,|\,(\mathcal{H}^2_{SO})^2\,|\,\Gamma_8(\tfrac{3}{2})\rangle_{diag} = \tfrac{3}{10}\langle\Gamma_6\,|\,\mathcal{H}^2_{SO}\,|\,\Gamma_6\rangle + \tfrac{1}{30}\langle\Gamma_7\,|\,\mathcal{H}^2_{SO}\,|\,\Gamma_7\rangle + \tfrac{41}{75}\langle\Gamma_8(\tfrac{3}{2})\,|\,\mathcal{H}^2_{SO}\,|\,\Gamma_8(\tfrac{3}{2})\rangle + \tfrac{3}{25}\langle\Gamma_8(\tfrac{5}{2})\,|\,\mathcal{H}^2_{SO}\,|\,\Gamma_8(\tfrac{5}{2})\rangle$$
$$-\tfrac{8}{25}\langle\Gamma_8(\tfrac{3}{2})\,|\,\mathcal{H}^2_{SO}\,|\,\Gamma_8(\tfrac{5}{2})\rangle,$$

$$\langle\Gamma_8(\tfrac{5}{2})\,|\,(\mathcal{H}^2_{SO})^2\,|\,\Gamma_8(\tfrac{5}{2})\rangle_{diag} = \tfrac{1}{30}\langle\Gamma_6\,|\,\mathcal{H}^2_{SO}\,|\,\Gamma_6\rangle + \tfrac{3}{10}\langle\Gamma_7\,|\,\mathcal{H}^2_{SO}\,|\,\Gamma_7\rangle + \tfrac{3}{25}\langle\Gamma_8(\tfrac{3}{2})\,|\,\mathcal{H}^2_{SO}\,|\,\Gamma_8(\tfrac{3}{2})\rangle + \tfrac{41}{75}\langle\Gamma_8(\tfrac{5}{2})\,|\,\mathcal{H}^2_{SO}\,|\,\Gamma_8(\tfrac{5}{2})\rangle$$
$$+\tfrac{8}{25}\langle\Gamma_8(\tfrac{3}{2})\,|\,\mathcal{H}^2_{SO}\,|\,\Gamma_8(\tfrac{5}{2})\rangle,$$

$$\langle\Gamma_8(\tfrac{3}{2})\,|\,(\mathcal{H}^2_{SO})^2\,|\,\Gamma_8(\tfrac{5}{2})\rangle_{diag} = -\tfrac{1}{10}\langle\Gamma_6\,|\,\mathcal{H}^2_{SO}\,|\,\Gamma_6\rangle + \tfrac{1}{10}\langle\Gamma_7\,|\,\mathcal{H}^2_{SO}\,|\,\Gamma_7\rangle - \tfrac{4}{25}\langle\Gamma_8(\tfrac{3}{2})\,|\,\mathcal{H}^2_{SO}\,|\,\Gamma_8(\tfrac{3}{2})\rangle + \tfrac{4}{25}\langle\Gamma_8(\tfrac{5}{2})\,|\,\mathcal{H}^2_{SO}\,|\,\Gamma_8(\tfrac{5}{2})\rangle$$
$$+\tfrac{6}{25}\langle\Gamma_8(\tfrac{3}{2})\,|\,\mathcal{H}^2_{SO}\,|\,\Gamma_8(\tfrac{5}{2})\rangle,$$

and

$$\langle t\tau J\,|\,\mathcal{H}^2_{SO}\,|\,t\tau J'\rangle_{off\text{-}diag} = \langle t\tau J\,|\,\mathcal{H}^2_{SO}\,|\,t\tau J'\rangle - \langle t\tau J\,|\,\mathcal{H}^2_{SO}\,|\,t\tau J'\rangle_{diag}.$$

[1] S. Koide and M. H. L. Pryce, Philos. Mag. 3, 607 (1958).
[2] A. D. Liehr and C. J. Ballhausen, Phys. Rev. 106, 1161 (1957).
[3] L. L. Lohr, Jr., J. Chem. Phys. 45, 3611 (1966).
[4] R. L. Greene, D. D. Sell, W. M. Yen, and A. I. Schawlow, Phys. Rev. Lett. 15, 656 (1965). See also a review paper by D. D. Sell, J. Appl. Phys. 39, 1030 (1968).
[5] E. I. Solomon and D. S. McClure, Phys. Rev. B 9, 4690 (1974); 6, 1697 (1972).
[6] M. Y. Chen, D. S. McClure, and E. I. Solomon, Phys. Rev. B 6, 1690 (1972); R. S. Meltzer, Marian Lowe, and D. S. McClure, Phys. Rev. 180, 561 (1969).
[7] D. H. Goode, J. Chem. Phys. 43, 2830 (1965).
[8] D. S. McClure, J. Chem. Phys. 39, 2850 (1963).
[9] D. Langer and S. Ibuki, Phys. Rev. 138, A809 (1965).
[10] R. Parrot and C. Blanchard, Phys. Rev. B 6, 3992 (1972).
[11] B. Lambert, T. Buch, and A. Geoffroy, Phys. Rev. B 8, 863 (1973).
[12] A. I. Schawlow, A. H. Piksis, and S. Sugano, Phys. Rev. 122, 1469 (1961).
[13] D. Langer and H. J. Richter, Phys. Rev. 146, 554 (1966).
[14] M. D. Sturge, in *Solid State Physics*, edited by F. Seitz, D. Turnbull, and H. Ehrenreich (Academic, New York, 1967), Vol. 20.
[15] F. S. Ham, Phys. Rev. 138, A1727 (1965).
[16] J. S. Griffith, *The Irreducible Tensor Method for*

Molecular Symmetry Groups (Prentice-Hall, Englewood Cliffs, 1962).
[17]The mixing of the two ^2D spectroscopic terms with seniority 1 and 5 by the electrostatic interaction complicates slightly the calculation of the matrix elements of the cubic crystal field within the ^2E and $^2T_1$ states.
[18]J. H. Van Vleck, J. Chem. Phys. 41, 67 (1937).
[19]Y. Tanabe and S. Sugano, J. Phys. Soc. Jpn. 9, 753 (1954).
[20]A. D. Liehr and C. J. Ballhausen, Mol. Phys. 2, 123 (1959).
[21]J. S. Griffith, *The Theory of Transition Metal Ions* (Cambridge U.P., Cambridge, England, 1961).
[22]J. S. Griffith, Mol. Phys. 3, 477 (1960).
[23]F. Rohrlich, Astrophys. J. 129, 441 (1959); 129, 449 (1959).
[24]B. R. Judd, Phys. Rev. 127, 750 (1962).
[25]G. S. Ofelt, J. Chem. Phys. 37, 511 (1962).
[26]B. R. Judd, *Second Quantization and Atomic Spectroscopy* (Johns Hopkins, Baltimore, 1967).
[27]B. G. Wybourne, in *Optical Properties of Ions in Crystals*, edited by H. M. Crosswhite and H. W. Moos (Wiley, New York, 1967).
[28]The levels $(^6A_1)\ \Gamma_7$ and $(^6A_1)\ \Gamma_8$ are separated by $23.6 \times 10^{-4}\,cm^{-1}$ for Mn^{++} in cubic ZnS and by $59.1 \times 10^{-4}\,cm^{-1}$ for Mn^{++} in ZnSe; J. Schneider, S. R. Sircar, and A. Raüber, Z. Naturforsch. A 18, 980 (1963).
[29]The contribution of the spin-spin interaction to the splitting of the $(^4T_2)\ \Gamma_6$ and $(^4T_2)\ \Gamma_8$ levels is less than $1.5\ cm^{-1}$, the $(^4T_2)\ \Gamma_6$ level being at lower energy.
[30]F. S. Ham, W. M. Schwarz, and M. C. M. O'Brien, Phys. Rev. 185, 548 (1969).
[31]F. S. Ham and G. A. Slack, Phys. Rev. 4, 777 (1971).
[32]B. Hennion, F. Moussa, G. Pepy, and K. Kunc, Phys. Lett. A 36, 376 (1971).
[33]J. T. Vallin and G. D. Watkins, Phys. Rev. B 9, 2051 (1974).
[34]B. Nygren, J. T. Vallin, and G. A. Slack, Solid State Commun. 11, 35 (1972).
[35]Don Berlincourt, H. Jaffe, and L. R. Shiozawa, Phys. Rev. 129, 1009 (1963).
[36]F. S. Ham, Phys. Rev. 166, 307 (1968).